Published in final edited form as:

*Cancer Res*. 2019 March 15; 79(6): 1151–1164. doi:10.1158/0008-5472.CAN-18-0779.

# Natural Killer-derived exosomal miR-186 inhibits neuroblastoma growth and immune escape mechanisms.

**Paolo Neviani**[1], **Petra M Wise**[1], **Mariam Murtadha**[1], **Cathy W Liu**[1], **Chun-Hua Wu**[1], **Ambrose Y Jong**[1], **Robert C Seeger**[1], and **Muller Fabbri**[1,2,*]

[1]Children's Center for Cancer and Blood Diseases and Divisions of Hematology, Oncology, Blood and Marrow Transplantation, Department of Pediatrics, The Saban Research Institute, Children's Hospital Los Angeles, USC-Norris Comprehensive Cancer Center, Keck School of Medicine, University of Southern California, Los Angeles, CA 90027, USA.

[2]Current Address: University of Hawai'i Cancer Center, Cancer Biology Program, University of Hawai'i at Mānoa, Honolulu, HI 96813, USA.

## Abstract

In neuroblastoma, the interplay between immune cells of the tumor microenvironment and cancer cells contributes to immune escape mechanisms and drug resistance. In this study, we show that NK cell-derived exosomes carrying the tumor suppressor microRNA (miR)-186 exhibit cytotoxicity against MYCN-amplified neuroblastoma cell lines. The cytotoxic potential of these exosomes was partly dependent upon expression of miR-186. MiR-186 was downregulated in high-risk neuroblastoma patients, and its low expression represented a poor prognostic factor that directly correlated with NK activation markers (i.e. NKG2D and DNAM-1). Expression of MYCN, AURKA, TGFBR1 and TGFBR2 was directly inhibited by miR-186. Targeted delivery of miR-186 to MYCN-amplified neuroblastoma or NK cells resulted in inhibition of neuroblastoma tumorigenic potential and prevented the TGFβ1-dependent inhibition of NK cells. Altogether, these data support the investigation of a miR-186-containing nanoparticle formulation to prevent tumor growth and TGFβ1-dependent immune escape in high-risk neuroblastoma patients as well as the inclusion of *ex vivo* derived NK exosomes as a potential therapeutic option alongside NK cell-based immunotherapy.

## Introduction

Neuroblastoma, the most common extracranial childhood cancer, is a malignancy of the embryonal sympathetic nervous system derived from highly proliferative migratory cells of the neural crest. It is characterized by a highly heterogeneous clinical behavior based on the patient's risk at the time of diagnosis, and response to treatment depends on several factors such as age, site of primary tumor, histology, lymph node involvement and biological features(1). Age at diagnosis is a strong prognostic factor, in fact, while children diagnosed

*Corresponding Author: Muller Fabbri, MD, PhD, 701 Ilalo Street, Room 338, Honolulu, HI 96813, USA. Phone: (808) 564-3804; Fax: (808) 587-0742; mfabbri@cc.hawaii.edu.

Competing Financial Interests Statement

The authors declare that they have no competing financial interests.

under 1 year of age show survival rates of up to 95%, this drops to 68% for children aged 1 to 14 years, and overall five-year survival for all patients, regardless of risk group, is 71%(2). Based on the International Neuroblastoma Staging System (INSS) patients can be stratified in 5 different risk groups (1, 2, 3, 4 and 4S) ranging from spontaneously regressing to highly malignant and metastatic tumors(3). Regardless of staging, the amplification of the oncogene MYCN, found in 25% of cases, is the single strongest biological marker predicting poor prognosis and drug resistance(4). MYCN expression has been found to positively correlate with metastatic behavior, epithelial mesenchymal transition (EMT), impaired immune surveillance, cell cycle progression and maintenance of a stem cell-like state(4). Because of its secondary structure and the lack of surfaces for small molecule binding, efforts in therapeutically targeting MYCN have been futile, and to date myc family proteins are considered undruggable, hence indirect targeting is currently under investigation(1,4). Among genes highly expressed in MYCN-amplified neuroblastoma, Aurora Kinase A (AURKA) is physically associated to MYCN and promotes its stability by inhibiting its proteasome dependent degradation(5). Therefore, AURKA has emerged as a potential target to promote MYCN down-regulation; indeed its targeting with shRNA or small molecules (e.g. MLN8237; CD532) resulted in MYCN degradation and has shown promising results in pre-clinical studies(5–7).

In an effort to overcome drug resistance in high-risk neuroblastoma, understanding the role of the tumor microenvironment is of extreme importance. Cancer cells are able to profoundly influence the biology of local immune cells, such as tumor associated macrophages and natural killer cells, by establishing immune escape mechanisms that inhibit the innate anti-tumoral immunity response and induce a pro-inflammatory and pro-tumoral microenvironment(8).

CD163+ tumor associated macrophages (TAM) are the most abundant stromal component in the neuroblastoma microenvironment and are known to produce immunosuppressive cytokines and several factors (e.g. TGFβ, IL-4, IL-10, VEGF) that support angiogenesis and metastatic potential(9). While high infiltration of TAMs at the tumor site has poor prognostic potential, by contributing to drug-resistance(9–11); abundance of activated NK cells in the tumor microenvironment cells is a favorable prognostic factor when their cytotoxic activity is sustained by a supportive cytokine profile(12). Unfortunately, in high-risk neuroblastoma, high levels of TGFβ1 have been detected in the microenvironment, causing suppression of the cytotoxicity of NK cells by downregulating the expression of cytotoxicity receptors (e.g. DNAM-1 and NKG2D) and altering their chemokine receptor repertoire (e.g. CXCR4, CXCR3, CX3CR1)(13–18). Furthermore, high local production of TGFβ1 and activation of the canonical (i.e. SMADs) and non-canonical TGFβ pathways (e.g. ROCK1, MAPK1) promote neuroblastoma invasiveness by inducing EMT(19–21). Therefore, given the increasing evidence of the role of the TME in tumorigenesis, it is important not only to identify cancer cell specific targets but also other microenvironment-associated factors that are responsible for the establishment of a drug resistant phenotype. In elucidating the role of NK cells in the interplay between cancer cells and the tumor microenvironment, it has been recently reported that exosomes derived from NK cells exert cytotoxic activity against cancer cells(22–24). Here we show that the cytotoxicity of NK exosomes depends not only on the presence of canonical killer molecules (i.e. Perforin 1, Granzyme A and B) but also

on their nucleic acid cargo. Interestingly, we and others have shown that miRs can be transferred between immune and cancer cells within the tumor microenvironment, and that these miRs may target factors important for tumorigenesis and the establishment of immune escape mechanisms(8,10). Here we show that the tumor suppressor miR-186 is present in NK-derived exosomes and that its expression is downregulated in high-risk neuroblastoma. Importantly, miR-186 is *in silico* predicted to target MYCN, AURKA and the TGFβ pathway. Ectopic delivery of miR-186 to neuroblastoma cells and to NK cells, impaired the survival and migration of MYCN-amplified neuroblastoma cells both *in vitro* and *in vivo* and prevented the TGFβ1-dependent inhibition of NK cytotoxicity. Importantly, NK-derived exosomes were able to efficiently kill MYCN-amplified neuroblastoma cells regardless of the activation status of the parental NK cells. Moreover, modulation of miR-186 abundance in these exosomes altered their cytotoxic potential, suggesting that miR-186 may be at least in part responsible for their cytotoxic activity and that NK exosomes may be insensitive to TGFβ1 dependent inhibition and may represent another viable strategy to overcome immune escape mechanisms in neuroblastoma.

## Methods

### Cell lines and primary cells

The MYCN-amplified, CHLA-136 and LAN-5 (obtained from the Children's Oncology Group), and non-amplified, CHLA-255 (described in(25)) human neuroblastoma cell lines were cultured in Iscove's Modified Dulbecco's *Medium* (*IMDM, Life Technologies)* containing either 10% heat-inactivated fetal bovine serum (FBS) (for CHLA-255), or 20% FBS (for CHLA-136 and LAN-5) supplemented with 50 U of penicillin/ml, and 0.1 mg of streptomycin/ml at 37°C in a 5% $CO_2$ humidified atmosphere. The CHLA-255-Fluc, CHLA-136-Fluc, LAN-5-Fluc, CHLA-136-miR-186 CHLA-miR-136-EV cells were generated by lentiviral transduction a firefly luciferase lentiviral vector. For NK cell propagation, peripheral blood mononuclear cells were Ficoll-isolated from healthy donors and co-cultured with irradiated (100 Gy) K562.mbIL21(26) at a 1:1 ratio in RPMI1640 with 10% FBS and 50U/ml of rhIL2 (PeproTech). K562.mbIL21 cells were replenished at day 7 and rhIL2 added every 3 days. At day 14 the purity of NK cells and T cell contamination were determined by CD56/CD16/CD3 immunostaining followed flow cytometry analysis (Supplementary Fig. 1a). The expanded NK cells were viably frozen at day 14. Frozen aliquots of NK cells were thawed and kept in the presence of 150U/ml rhIL2 for at least 24h, then washed three times in PBS and starved for at least 24h before addition of 100 ng/ml of rhIL15 and/or exposure to CD56-coated miR-186-loaded nanoparticles. All cells were tested to be Mycoplasma free before performing experiments. All cells were kept in culture for 24–48h after splitting and before doing any experiments, so that they had time to adhere to the bottom of the flask. When they reached 80% confluence, experiments were performed with the indicated timing.

### Transfection and Lentiviral Transduction

The miR-186–5p mimic (MC11753) and inhibitor (MH11753), and corresponding negative controls (Life Technologies) were packaged into artificial exosomes using DOTAP transfection reagent (Roche) according to the manufacturer's protocol. Lentiviral

pseudotyped particles were produced by Lipofectamine 2000 (Life Technologies) mediated transfection of 293TN cells (System Biosciences) with the lentiviral vector, the psPAX2 packaging construct (gift from Dr Didier Trono, addgene plasmid #12260), and a plasmid carrying the G-glycoprotein of vesicular stomatitis virus (VSV-G). Viral supernatant was collected 36h post transfection and filtered through a 0.45μm membrane. Cells were incubated for 6h with the viral supernatant and 8 μg/ml of Hexadimethrine bromide (Sigma-Aldrich) and FACS-sorted 48h post transduction.

## Immunoblotting

Cells were lysed in RIPA buffer (150 mM NaCl, 1% NP-40, 0.1% SDS, 50 mM Tris [pH 8.0]) supplemented with 1μg/ml Aprotinin, 1mM DTT, 0.2mM PMSF 1μg/ml pepstatin A. The protein concentration was determined by Bradford Protein Assay (BioRad) and equal amount of proteins were resolved by SDS gel electrophoresis, transferred to a nitrocellulose membrane and subjected to a standard immunoblotting protocol. For the analysis of SEC eluted fractions, the proteins were isolated by Trichloroacetic Acid (Sigma-Aldrich) precipitation followed by acetone washes of the protein pellets. Precipitated proteins were re-suspended directly in Laemmli Sample buffer and resolved by SDS gel electrophoresis. The antibodies used were: rabbit polyclonal anti-Aurora A/AIK #3092, rabbit monoclonal anti-SMAD3 #9523, anti-SMAD2 #5339 (Cell Signaling); mouse monoclonal anti-Tsg101 sc-7964, anti-TGFβ RII sc-17791, anti-Fibronectin sc-8422, anti-Perforin 1 sc-373943, anti-HSP70 sc-24, anti-Alix sc-53540 and rabbit polyclonal anti-calnexin sc-11397 (Santa Cruz Biotechnology, Inc.); mouse monoclonal anti-MYCN Ab16898 and rabbit polyclonal anti-TGFβ RI Ab31013 (abcam); rabbit polyclonal anti-CD81 EXOAB-CD81A-1 (System Biosciences); mouse monoclonal anti-Granzyme A #507202 and anti-Granzyme B #674302 (Biolegend).

## RNA isolation and qPCR

Total RNA was extracted from cells and exosomes using Trizol reagent (Invitrogen). Reverse transcriptions were performed using iScript cDNA Synthesis Kit (Biorad) for mRNA expression, and the TaqMan miRNA Reverse Transcription kit (Life Technologies) for mature miR expression. Quantitative real-time PCR (qPCR) of miRs was performed using commercially available TaqMan MicroRNA Assay primers and probes. For mRNA qPCR, previously validated primer pairs were identified on the PrimerBank database (https://pga.mgh.harvard.edu/primerbank/index.html) and used in SYBR green chemistry based qPCR protocols. All qPCR analyses were performed on a CFX96 Touch™ Real-Time PCR Detection System (BioRad) with iTaq Universal SYBR Green Supermix (BioRad) or TaqMan Fast PCR Advanced Master Mix (Life Technologies) for mRNA or miRs expression analysis, respectively. Relative mRNA or miR expression levels were calculated using the $2^{-\Delta\Delta C\tau}$ method and normalized by expression levels of GAPDH mRNA or of U6 snRNA, respectively. For exosomal RNA, levels of miR expression were normalized by total amount of RNA and reported as $2^{-C\tau}$. Primer sequences are reported in Supplementary Table 1.

## Luciferase reporter assays

For the luciferase reporter assays we used the CHLA-255 neuroblastoma cell line: $2\times10^6$ cells in 200μl were transfected with the indicated reporter plasmids and miR-186 or

scrambled control at a final concentration of 100nM. Transfections were carried out by electroporation in a GenePulser Xcell electroporation system (BioRad) with the following settings: exponential; 250V, 975uF, ∞ Ω, 4mm. Transfected cells were then incubated for 48h and both firefly and renilla luciferase activities were assessed using the Dual-Luciferase Reporter Assay protocol in a GloMax Multi+ luminometer (Promega). The Renilla luciferase activity was normalized by firefly luciferase activity and expressed as change relative to the value of the negative control, which was set as 1.

### Growth curves

$25–50\times10^3$ neuroblastoma cells/well were seeded in a 12-well plate; after overnight incubation, the cells were transfected with 100nM of scrambled or miR-186 mimic in triplicates in IMDM with 1% BSA. Viable Cells were detected by trypan blue dye exclusion assays and counted with a TC10 automated cell counter (BioRad) at the indicated time points.

### Migration and wound-healing assay

$1\times10^5$ LAN-5 cells transfected with 100nM of scrambled or miR-186 mimic were seeded on top of 8μm polyethylene terephthalate (PET) transwell inserts. Migration assays were carried out in 2% FBS/IMDM. SDF1α (100ng/ml) was added to the bottom well. After 4h, the top side of the transwell was wiped to remove non-migrated cells and the migrated cells were stained with the Protocol® Hema 3 staining kit (Fisher HealthCare). Stained membranes were mounted on slides, and visualized at a 10x magnification; 9 representative fields per membrane were acquired and the number of cells was averaged across three replicates.

For the wound-healing assay, LAN-5 or CHLA-136 cells were grown to confluence in 6-well plates and transfected with 100nM of scrambled or miR-186 mimic. The monolayers were scratched with a pipette tip and cultured for 6 days. Images of the scratches were acquired at time 0, and at 3 and 6 days (4 fields/well) and the average distance of cell migration determined by ImageJ software. The migration rate was expressed as the size of the scratch after 6 days in culture relative to the size at time zero.

### Flow Cytometry analysis

Cells were stained with the following antibodies: PE anti-GD2, PE/Cy7 anti-CD56 (NCAM), PE anti-CD16 (3G8), FITC anti-CD3 (HIT3a) (Biolegend); PE anti-CXCR4 (BD Biosciences). Stained cells were analyzed in a BD LSR II flow cytometer (BD Biosciences).

### Imaging Flow Cytometry

The RNA cargo of NK exosomes was stained with the SYTO RNASelect Green Fluorescent dye and the excessive unincorporated dye was removed with Exosome Spin Columns following the manufacturer’s protocol (ThermoFisher). CHLA-136 and LAN-5 cells were exposed to stained and NK exosomes for 18 hours and acquired on the Imagestream X Mark II imaging flow cytometer and analyzed with the IDEAS software (Amnis corporation). Cells were visualized at a 40X magnification and excited with a 488nm laser; the emission

from internalized exosomes was detected by 533/55 bandpass filter and bright-field images were used to determine the cell boundaries.

## Constructs and mutagenesis

**psiCHECK-2 luciferase reporter vectors.—**Potential miR-186 target sequences were *in silico* predicted at https://www.microRNA.org or https://www.targetscan.org. The full length 3'UTRs of MYCN, AURKA and fragments (containing a potential miR-186 target sequence) of TGFBR1 (nucleotides 3551–4166), SMAD2 (nucleotides 601–821) and SMAD3 (nucleotides 843–1037; 1357–1573 and 2278–2508) 3'UTRs were PCR-amplified from LAN-5 genomic DNA and cloned between the XhoI and NotI restriction sites of the psiCHECK-2 dual luciferase reporter vector (Promega), cloning primer sequences are reported in Supplementary Table 1. The psiCHECK-2-TGFBR2–3UTR-WT construct was a gift from Robert Blelloch (Addgene plasmid # 31882) (27). The miR-186 7/8-mer seed regions in the 3'UTRs of MYCN, AURKA, TGFBR1 and TGFBR2 were deleted with the QuikChange II XL Site-Directed Mutagenesis kit (Agilent).

**pSBE4.—**The SBE4-Luc smad-reporter plasmid was a gift from Bert Vogelstein (Addgene plasmid # 16495)(28).

**Lentiviral pCDH vectors.—**The human full-length MYCN and AURKA were PCR-amplified from LAN-5 cDNA and cloned between the XbaI and EcoRI sites of the pCDH-CMV-MCS-EF1-copGFP (CD511B-1) lentiviral vector (System Biosciences).

## Anti-CD56 or anti-GD2 antibody conjugated Anionic Lipopolyplex nanoparticles

The preparation of antibody-conjugated nanoparticles has been previously described(29). The DSPE-PEG2000 maleimide conjugated antibodies used to coat the surface of the lipopolyplex nanoparticles were: LEAF purified anti-CD56 (clone HCD56, 318324, Biolegend) and chimeric anti-GD2/ch14.18 (United Therapeutics Corp).

## NK exosome isolation by Size Exclusion Chromatography

For NK exosome preparation, NK cells were cultured for 48h in 10% FBS/RPMI medium that had been cleared of bovine exosomes by an ultracentrifugation step for 1h at 100,000g. The supernatant was centrifuged at 300g for 10 minutes, followed by centrifugation at 3000g for 10 minutes. The clarified supernatant was then concentrated to approximately 500μl on a 100KD Amicon Ultra Centrifugal filter (Millipore). The NK exosomes were then isolated from the concentrated supernatant by size exclusion chromatography (SEC). Sephacryl S-300 High Resolution (GE Healthcare) was packed on a glass econo-column chromatography column (BioRad) (10cm height, 1.5cm diameter). The column was washed with 0.32% Sodium Citrate in PBS and the supernatant was loaded onto the column and allowed to enter the resin by gravity flow. The eluate was collected in 23 fractions of 15 drops (~500μl) on a Model 2110 Fraction Collector (BioRad). For each fraction, the presence of exosomes was determined by nanoparticle tracking analysis, protein concentration and anti-CD81, anti-Calnexin, anti-TSG101, and anti-Fibronectin immunoblotting. The exosome-containing fractions were then further concentrated to $1/100^{th}$ of the original supernatant.

### Transmission Electron Microscopy

Exosomes isolated by size exclusion chromatography were precipitated with ExoQuick (System Biosciences) following the manufacturer instruction, to obtain a discreet pellet. Pelleted exosomes were immediately fixed in 2.5% glutaraldehyde. The exosomes were then post-fixed with 1% Osmium Tetroxide, dehydrated with alcohols, embedded in a mold with eponate resin and cured overnight in an oven. Ultra-thin (80–100nm) sections were cut at with a diamond knife, and onto copper grids with formvar. The grids are stained with uranyl acetate and lead citrate to give the images more contrast. Samples were imaged with a FEI Morgagni transmission electron microscope with Olympus imaging software.

### NK cytotoxicity assay

Frozen aliquots of 15-day-old K562.mbIL21-expanded aNK cells were thawed and cultured in 10% FBS/RPMI1640 with 150U/ml of rhIL-2 for at least 48h. For the cytotoxicity assays, NK cells were washed twice in PBS and starved from growth factors in 10% FBS/RPMI1640 for 24h. NK cells were then treated with 100ng/ml of rhIL-15, and/or 10ng/ml of rh TGFβ1, and/or anti-CD56 labeled miR-186 carrying nanoparticles. The cytotoxicity was assessed by seeding CHLA-136-Fluc cells ($20\times10^3$ cell/well) into individual wells of a 96-well plate together with a 2-fold serial dilution of aNK cells, starting with an NK:NB ratio of 10:1. After a 6h incubation at 37C, survival was assessed by adding D-luciferin to individual wells, and the luminescence acquired by a Promega GloMax-multi microplate reader. For the NK exosome cytotoxicity assay the same protocol was performed with the exception that a 2-fold serial dilution of freshly isolated NK exosomes (starting at $4\times10^{11}$ particles/ml) were seeded in the presence of $10\times10^3$ cells/well CHLA-136-Fluc cells.

### Nanoparticle Tracking Analysis (NTA)

NTA analysis was performed on a NanoSight NS300 instrument (Malvern) as previously described(10).

### *In vivo* orthotopic neuroblastoma mouse model

All animal experiments were performed as approved by the Institutional Animal Care and Usage Committee (IACUC) of Children's Hospital Los Angeles. The orthotopic xenograft neuroblastoma mouse model has been described in(13). 4 to 8-week old female and male NSG (NOD.Cg-*Prkdc*$^{scid}$ *Il2rg*$^{tm1Wjl}$/SzJ) mice were intra-renally transplanted with $1\times10^6$ CHLA-136-Fluc cells in the left kidney. Tumor growth was monitored by bioluminescence imaging using a Xenogen IVIS 200 instrument (Perkin-Elmer). Tail-vein injections of nanoparticles were started 4 days after transplantation and carried out three times weekly at a dose of RNA of 1mg/Kg/die as described in(29). The RNA oligos for *in vivo* experiments were purchased from Bio-Synthesis. Mice were euthanized 30 days post transplantation, and tumors and contralateral kidneys were excised, weighed and homogenized; the expression of miR-186 in livers was detected as a non-GD2 expressing tissue control. For survival studies mice were treated for up to 60 days and humanely euthanized according to the IACUC guidelines.

### Statistical Analysis

Statistical data are presented as mean ± standard deviation. Statistical significance was calculated by two-tailed Student's *t* test. The survival analysis was calculated by the Kaplan-Meier method, and the log-rank test. The GraphPad Prism version 6.0h software was used for statistical analyses.

## Results

### NK cells secrete cytotoxic exosomes that carry miR-186

NK cells were isolated and expanded from the peripheral blood from healthy donors and their purity confirmed by immunophenotyping after 14 days in co-culture with the feeding cell line K562.mbIL21 (Supplementary Fig. 1a). To isolate extracellular vesicles the supernatant of NK cells was concentrated and processed by size exclusion chromatography (SEC). The presence of extracellular vesicles in the SEC fractions was confirmed by nanosight tracking analysis (Fig. 1a, left). Most particles were detected in fractions 13 and 14, had a median diameter of 92.45 nm, and had a structure revealed by transmission electron microscopy consistent with the expected size and morphology of exosomes (Supplementary Fig. 1b)(30). Moreover, immunoblots were performed to further characterize the particles following the guidelines of the International Society of Extracellular Vesicles(30). Accordingly, NK-derived exosomes were positive for the tetraspanin transmembrane marker CD81, the cytosolic proteins TSG101 and HSP70, the endosomal associated protein ALIX and the extracellular protein Fibronectin and negative for the intracellular protein Calnexin, used as a cell contamination marker (Fig. 1a, right).

When assessed in cytotoxicity assays, IL-15 activated NK cells and their exosomes were able to kill neuroblastoma cells in a dose dependent manner (Fig. 1b); interestingly while the cytotoxicity of NK cells starved from growth factors or treated with TGFβ1 was inhibited, their exosomes showed killing equal to exosomes derived from activated NK cells (Fig. 1b). Notably, exosomes derived from inactivated NK cells had low levels of the killer molecules Perforin 1, Granzyme A and Granzyme B, while still retaining their cytotoxic activity (Fig. 1c), suggesting that the cytotoxic activity of NK exosomes may be in part dependent on other factors (e.g. exosomal miRs and/or mRNAs) other than on classical NK cytotoxic proteins. To prove that the exosome-dependent cytotoxicity is NK-exosome specific and not due to carryover of K562.mbIL21 derived exosomes; K562 were isolated and tested in cytotoxicity assays: as expected the exosomes derived from this unrelated, non-cytotoxic, myeloid leukemia cell line did not exert any cytotoxic effect on target cells, compared to exosomes derived from IL-15 activated NK cells (Fig. 1d).

To elucidate the potential role of the miR payload in NK exosomes we profiled the top miRs represented in the NK exosomes. Among these, the tumor suppressor miR-186–5p (NR_029707) was predicted *in silico* to target factors important for the survival of neuroblastoma cells (e.g. MYCN and AURKA) and several components of the TGFβ-pathway (e.g. TGFBR1, TGFBR2, SMAD2, SMAD3) (Table 1), which is involved in the TGFβ-dependent inhibition of NK cytotoxicity, a common immune escape mechanism in neuroblastoma.

## miR-186–5p expression is low in high-risk and MYCN amplified neuroblastoma and correlates with the expression of NK activation markers

Since miR-186 has been previously described as a tumor suppressor, we evaluated its expression in a publicly available RNA-seq dataset containing 498 primary neuroblastoma samples (FDA SEQC NB) with the R2: Genomics Analysis and Visualization Platform (http://r2.amc.nl)(31). Patients were stratified by risk (high-risk: stage 4 disease in patients older than 18 months at diagnosis and patients of any age and stage with MYCN-amplified tumors), by MYCN-status, or by INNS ranking(32). We found miR-186 expression to be significantly down-regulated in high versus low-risk, MYCN-amplified versus non-amplified and stage 4 versus the lower risk stages (Fig. 2a). Remarkably, patients with low expression of miR-186 showed significantly shorter event-free survival and overall survival probability, consistent with a role miR-186 as a *bona fide* tumor suppressor (Fig. 2b)(33–41).

In another publicly available dataset (GEO#: GSE16237), RNA from 51 neuroblastoma samples was analyzed by Affymetrix array and miR-186 was found to positively correlate with the NK activation markers NKG2D and DNAM-1 (Fig. 2c), suggesting that high expression of miR-186 may be associated with the presence of activated NK cells in neuroblastoma. Moreover, analysis of the expression of NKG2D and DNAM-1 revealed that their expression is significantly down-regulated in the higher risk categories of neuroblastoma and that their low expression is a poor prognostic factor in neuroblastoma (Supplementary Fig. 1C), underscoring the importance of NK cell activation in the neuroblastoma microenvironment. Interestingly, significantly lower expression of miR-186 was detected in TGFβ-treated NK cells compared to IL-15 activated NK cells (Fig. 2d), suggesting that the expression of miR-186 may be inhibited by TGFβ signaling and may correlate with TGFβ-regulated NK cytotoxicity. Moreover, we confirmed that NK-exosomes carry miR-186 (Fig.2e) and deliver their RNA cargo (including miR-186) to the MYCN amplified neuroblastoma cell lines CHLA-136 and LAN-5 (Fig 2f, g). Interestingly, when CHLA-136 and LAN-5 cells were exposed to control K562.mbIL21 exosomes we did not see an increase of miR-186 suggesting that this miR-186 is specifically delivered by NK exosomes and not by exosomes derived from the feeding K562.mbIL21 cells (Fig 2g).

## miR-186–5p targets neuroblastoma oncogenes

To evaluate the role of miR-186 in MYCN-amplified neuroblastoma, we transiently transfected a mimic miR-186 or a scrambled sequence into the MYCN-amplified CHLA-136 or LAN-5 cell lines by treatment with artificial exosomes (Dotap-miR-186 or Dotap-Scr). Elevated miR-186 expression was detected up to 72 hours post-transfection compared to the scrambled control (Supplementary Fig. 2a). We then found that ectopic expression of miR-186 was inducing downregulation of the miR-186 predicted targets MYCN, AURKA, TGFBR1, TGFBR2 at protein but not mRNA level (Fig. 3a and Supplementary Fig. 2b). Thus, to assess whether miR-186 could directly prevent their mRNA translation, we performed luciferase reporter assays in the easily transfectable CHLA-255 neuroblastoma cell line. Notably, the expression of the luciferase reporter was inhibited upon miR-186 transfection when the wild-type 3’UTRs of MYCN, AURKA, TGFBR1 and TGFBR2 were cloned downstream of the renilla luciferase cDNA (Fig. 3b).

Importantly, when the predicted seed sequence was deleted from the 3'UTRs, the inhibitory effect of miR-186 was lost, indicating that miR-186 directly recognizes the target sequence and prevents MYCN, AURKA, TGFBR1 and TGFBR2 translation (Fig. 3b and Supplementary Fig. 2c). Next, to evaluate whether direct miR-186 dependent downregulation of TGFBR1, TGFBR2 was sufficient to inhibit TGFβ1-dependent signaling we employed a Smad-reporter assay and found that TGFβ1 was unable to induce Smad-dependent transcription in cells that had been transfected with miR-186 (Fig. 3c)(28).

To further demonstrate the direct targeting of MYCN and AURKA by miR-186 in neuroblastoma cells, we cloned their coding sequence lacking the 3'UTR into a lentiviral vector and transduced CHLA-136 and LAN-5 cells; in both cell lines the lack of 3'UTR was sufficient to rescue the expression of MYCN or AURKA when the cells were transfected with Dotap-miR-186 (Fig. 3d).

## Ectopic expression of miR-186 inhibits the growth and migration of MYCN-amplified neuroblastoma cell lines

To investigate the functional role of miR-186 in neuroblastoma we ectopically expressed miR-186 in CHLA-136 and LAN-5 cells. Cells transfected with dotap-miR-186 showed a significant reduction of their proliferation compared to dotap-scr cells (Fig. 4a). Furthermore, miR-186 transfected cells showed significantly impaired migration in wound healing assays (Fig. 4b) and reduction of migration in response to SDF1α (Fig. 4c) in Boyden chamber migration assays. Notably, the latter assays were performed only with LAN-5 because CHLA-136 cells do not express the SDF1α receptor CXCR4 (Supplementary Fig. 3a). The effect of miR-186 on the migration potential of neuroblastoma cells *in vitro* suggests a potential role for this miR in the epithelial to mesenchymal transition (EMT). Indeed, we found that genes involved in EMT (i.e. MMP12 and Vimentin) were downregulated following miR-186 expression in neuroblastoma cells (Fig. 4d).

## A nanoparticle modulating miR-186 in NK cells counteracts the TGFβ-dependent immune escape mechanism in neuroblastoma

Since we showed that miR-186 expression is low in high-risk neuroblastoma patients and that its expression may correlate with the activation of NK cells, we sought to investigate its role in the biology of NK cells. To efficiently transfect NK cells, we utilized anionic lypopolyplex nanoparticles (NP), a liposomal formulation that has been previously successfully utilized to transduce synthetic miRs or antagomiRs in human primary cells with high efficiency both *in vitro* an *in vivo*(29,42). Importantly, these nanoparticles have been shown to direct their cargo to specific target cells when labeled with an appropriate pegylated antibody(42). Nanoparticles coated with an anti-CD56 or an unrelated IgG were loaded with the miR-186 mimic or a scrambled control and exposed to NK cells *in vitro*, as expected, CD56 significantly and specifically enhanced the delivery of miR-186 in the target NK cells, compared to IgG-NP (Fig. 5a). We also utilized CD56-NPs carrying an anti-miR-186 antagomiR and found that expression of miR-186 was significantly reduced in the target cells (Fig. 5a). Importantly, a significant upregulation and downregulation of miR-186 was also detected in the corresponding NK exosomes (Fig. 5a).

We then investigated whether upregulation of miR-186 was able to target the TGFβ-pathway in NK cells and we found that upon CD56-NP-miR-186 treatment TGFBR1, TGFBR2, and SMAD3 were downregulated in the NK cells, suggesting that miR-186 is able to efficiently inhibit TGFβ signaling in activated NK cells (Fig. 5b).

Indeed, while TGFβ treatment was inhibiting the cytotoxicity of IL-15 activated NK cells treated with CD56-NP-Scr, TGFβ was unable to inhibit NK cells treated with CD56-NP-miR-186 (Fig. 5c), supporting the hypothesis that delivery of miR-186 to NK cells may circumvent the TGFβ-dependent immune escape mechanism in high-risk neuroblastoma and restore NK cytotoxicity in patients. To investigate the role of miR-186 in the cytotoxicity of NK exosomes we isolated NK exosomes from the supernatant of NK cells treated with CD56-NP-anti-miR-186 or CD56-NP-anti-Scr and found their cytotoxicity to be significantly impaired when miR-186 was downregulated, supporting a role for this miR in the cytotoxicity of these vesicles alongside other known cytotoxic factors such as perforin 1, granulysin and granzyme B (Fig. 5d)(22).

## Targeted delivery of miR-186 in an *in vivo* orthotopic model of neuroblastoma impairs the growth of cancer cells and improves survival

Having shown that forced expression of miR-186 in MYCN-amplified neuroblastoma cell lines effectively impaired their proliferation and migration potential, we sought to determine whether delivery of this miR *in vivo* could represent a possible new anti-cancer strategy. We utilized an orthotopic mouse model of neuroblastoma, in which we surgically injected the GD2-positive and MYCN-amplified CHLA-136-Fluc cells in the left kidney of NSG mice and started treatment four days later. As treatment, we utilized anti-GD2 coated NPs to specifically deliver the mature miR-186 to cancer cells. These NPs have been previously shown to have high bioavailability and a good safety profile in immune competent mice(29). We first tested these NPs *in vitro* and found that miR-186 was specifically delivered to CHLA-136-Fluc cells by GD2-NP-miR186 compared to the IgG-NP-miR-186, GD2-NP-Scr and IgG-NP-Scr controls (Supplementary Fig. 3b).

In a first *in vivo* experiment, 19 tumor-bearing mice were randomized and treated with IgG-NP-Scr ($n$=5) IgG-NP-miR-186 ($n$=4), GD2-NP-Scr ($n$=5) and GD2-NP-miR186 ($n$=5) intravenously three days a week. Tumor growth was monitored weekly by *in vivo* imaging for 30 days after transplantation and we found that (after 26 days of treatment) the luminescent signal from the mice treated with GD2-NP-miR186 was significantly lower compared to all control groups (Fig. 6a). Importantly, mice treated with GD2-NP-miR186 had significantly longer survival (median: 60 days) compared to mice treated with IgG-NP-Scr (median: 45 days), IgG-NP-miR-186 (median: 47 days), and GD2-NP-Scr (median: 52 days). Two identical independent *in vivo* experiment were then performed with the same treatment groups as above (all groups, *n=10 total each group*), images were taken 24 days after transplantation and all mice were euthanized 30 days post-surgery, tumor bearing kidneys were weighed and the tumors derived from mice treated with GD2-NP-miR186 showed markedly lower weight and size (Fig. 6b, left, and Supplementary Fig. 4). Furthermore, tumor bearing kidneys and the contralateral healthy kidneys were homogenized to extract RNA and analyze the expression of miR-186 by qPCR; as expected

miR-186 was efficiently and specifically delivered by GD2-NP-miR186 to the tumor site and not to the healthy kidney when compared to control groups (Fig. 6c, middle and right).

## Discussion

In order to successfully eradicate malignancies and overcome drug resistance a two-pronged approach is required: 1) directly targeting of the cancer cells to lead to efficient eradication of the primary tumor and 2) dissecting the biology of the tumor supportive microenvironment to negate pro-tumoral and pro-metastatic mechanisms(8,43). In high-risk neuroblastoma, the MYCN amplification found in cancer cells represents a major, yet undruggable, culprit and the targeting of its physically related partner, Aurora Kinase A, has shown promising pre-clinical results(4–6). Several TME dependent mechanisms of drug resistance have been described in neuroblastoma; for example, TAM-derived exosomes deliver miR-155 to neuroblastoma and induce drug resistance by downregulating the telomerase inhibitor TERF1(10); high infiltration of TAMs and elevated local production of the inflammatory cytokine IL-6 by monocytes has been reported to contribute to a pro-metastatic phenotype and to induce drug resistance(44). Importantly, elevated IL-6 and TGFβ expression in the tumor microenvironment activated the STAT3 and SMAD2/3 pathways in NK cells and suppressed activation of NK cell cytotoxicity, and IFNγ, granzymes A and B secretion, and perforin expression and has been reported to induce inhibition of the innate anti-tumor activity of NK cells(13,14). NK cells infiltrate the neuroblastoma microenvironment. Metelitsa et al., showed that 53% of primary neuroblastomas were infiltrated with CD1d-restricted Vα24-Jα18-invariant NK cells (iNKTs), and were most abundant in MYCN nonamplified tumors expressing CCL2(45). While the distribution of NK cells in relation to other immune cells within the neuroblastoma microenvironment is currently unknown, NK cells are specialized for the killing of cancer cells and clinical trials are ongoing to test NK cell-based therapy for the treatment of several malignancies, including neuroblastoma. The existence of an immune-suppressive microenvironment in neuroblastoma is relevant not only because it induces inhibition of the innate anti-tumor response of NK cells but also because it could hinder the efficacy of antibody-based therapies that rely on antibody-dependent cellular cytotoxicity (ADCC) mediated by NK cells(14,44). Moreover, we and others have recently reported that exosomes derived from NK cells expanded *in vitro* can be isolated in large quantities, contain NK markers and killer proteins and show cytotoxic activity against a variety of cancer cell lines (i.e. the murine melanoma cell line B16F10 and 501mel, the leukemia and lymphoma cell lines Jurkat, K562 and DAUDI and the breast cancer cell line SKBR3)(22–24). Here we show that exosomes derived from growth-factor starved or TGFβ inactivated NK cells retain their cytolytic activity, suggesting that factors other than NK specific killer molecules, such as their nucleic acid cargo, may be also required for their targeting activity (Fig. 1b,c). In this study, we focused on the potential role of exosomal miRs. Notably, extracellular miRs can be transferred between immune and cancer cells within the tumor microenvironment and they may have a role in targeting factors important for the survival and propagation of cancer cells and for the establishment of immune escape mechanisms(8,10). As global regulators of gene expression, miRs can simultaneously target multiple genes and have often been shown to be dys-regulated in cancer and specifically in

neuroblastoma(46). Among the miRs highly represented in the NK exosome cargo we found the tumor suppressor miR-186 (Table 1 and Fig. 2e). In a 2007 study of the prognostic relevance of miR expression in neuroblastoma Chen et al. showed that miR-186 is downregulated in MYCN-amplified tumors. This miR has been recently shown to behave mainly as a tumor suppressor in prostate cancer (targeting YY1 and CDK6)(47), in renal cell carcinoma (targeting SENP1)(48), in cervical cancer (competing with the oncogenic lncRNA ANRIL)(49), in non-small cell lung cancer (targeting MAP3K2 and ROCK1) (35,39), in hepatocellular carcinoma (targeting YAP1)(36), in multiple myeloma (targeting Jagged1)(37), in esophageal squamous cell carcinoma (targeting SKP2)(38) and in glioblastoma multiforme (targeting FGF2 and RelA)(41). Limitations of this study are related to the multiplicity of targets for a given miR, and the plethora of miRs contained as a cargo of extracellular vesicles. While our data support a role for miR-186 as a *bona fide* tumor suppressor in neuroblastoma, miR-based treatment approaches are hindered by the promiscuity of miR target genes. Moreover, further studies are necessary to study the reciprocal interactions of exosomal miRs within each other and how such interactions affect the phenotype of the recipient cells. Of note, a few studies have reported miR-186 as an onco-miR by inducing repression of FOXO1 in endometrial cancer, of CYLD in melanoma and of FAM134B in colorectal cancer(50–52). In this study, we show that in neuroblastoma miR-186 is downregulated in high-risk patients and its low expression represents a poor prognostic factor (Fig. 2a,b). Moreover, its levels directly correlate with the expression of two NK activation markers NKG2D and DNAM-1, whose low expression in neuroblastoma is dependent on the activation of the TGFβ signaling pathway (Fig. 2c)(16). Importantly, mir-186 was predicted *in silico* to target MYCN, AURKA the TGFβ pathway (Table 1 and Supplementary Fig. 2c)(22). Here, we show that mir-186 directly recognizes a seed sequence in the 3'-UTR of MYCN, AURKA, TGFBR1 and TGFBR2 mRNAs and induce downregulation of the encoded proteins and of the TGFβ pathway in the MYCN-amplified CHLA-136 and LAN-5 cells (Fig. 3 and Supplementary Fig. 2). Consistent with the role of miR-186 as a tumor suppressor, ectopic expression of this miRNA resulted in impaired *in vitro* proliferation of MYCN-amplified cell lines and inhibition of their migration potential (Fig. 4a,b). Forced expression of mir-186 also resulted in downregulation of MMP12 and Vimentin. Interestingly, serum MMP12 is a negative prognostic marker in cancer and has been previously shown to be induced by TGFβ1 and to correlate with enhanced tumor invasiveness(53,54). Moreover, Vimentin, a mesenchymal marker of metastatic potential is also induced by TGFβ, suggesting that inhibition of the TGFβ pathway by miR-186 in neuroblastoma cells may hinder the EMT process (Fig. 4b,c,d)(54). Furthermore, we show that *in vivo* targeted delivery of miR-186 to neuroblastoma cells is feasible by packaging in liposome-based nanoparticles coated with an anti-GD2 antibody. The *in vivo* administration of these anionic nanoparticles has been previously investigated in preclinical models of acute myeloid leukemias and found to have promising safety profile(29,42). Delivery of miR-186 to the GD2-positive CHLA-136 cell lines (Fig. 6a and Supplementary Fig. 2) implanted in an orthotopic model of neuroblastoma resulted in specific delivery of mir-186 to the tumor bearing kidney with significant reduction of tumor burden and enhanced survival (Fig. 6).

Since we showed that miR-186 was detected in the cytotoxic exosomes derived from activated NK cells and that this miR induces inhibition of TGFβ signaling by

downregulating TGFBR1 and TGFBR2 (Fig. 2 and 3), we sought to identify the role of miR-186 in NK cells. By utilizing nanoparticles coated with an anti-CD56 antibody, we delivered the mimic miR-186 and its inhibitor to NK cells, and consequently their exosomes, and confirmed downregulation of the TGFβ receptors when miR-186 is overexpressed (Fig. 5a,b). Importantly, ectopic expression of miR-186 in NK cells prevented the inhibition of their cytotoxicity upon treatment with TGFβ (Fig. 5c), suggesting that delivery of this miR to tumor sites may not only inhibit the growth of the neuroblastoma cancer cells, but also counteract the TGFβ-dependent immune escape mechanism that hampers the efficiency of ADCC-based therapies. Importantly, while the exosomes derived from activated NK cells showed significant cytotoxic activity against the CHLA-136 MYCN-amplified cell line, the exosomes derived from NK cells inactivated by growth-factor withdrawal or TGFβ treatment retained their cytotoxic activity (Fig. 1b). Interestingly, NK exosomes derived from growth-factor starved or TGFβ-treated NK cells showed a reduction in killer molecules (e.g. perforin 1, granzyme A and B), but retained equal levels of miR-186 suggesting that this miR (and potentially other RNA molecules carried by exosomes) may have a fundamental role in mediating the cytotoxicity of NK-derived exosomes. Accordingly, when miR-186 expression was inhibited in the exosomes after treatment of the parental NK cells with an anti-miR-186, their cytotoxic activity was significantly reduced (Fig. 5d).

In conclusion, we have provided evidence that targeted delivery of miR-186 in high-risk neuroblastoma is feasible and may lead to inhibition of tumor growth and spreading, and evasion of a common immune escape mechanism by which the tumor itself is able to circumvent the innate ability of NK cells to target cancer cells. Interestingly, while the use of anti-GD2 antibody is common in the treatment of neuroblastoma, the CD56 antigen is expressed by both neuroblastoma cells and NK cells, suggesting that this marker may be used to concurrently deliver miR-186 to NK and to the cancer cells(55). Moreover, the discovery that NK exosomes are cytotoxic and retain their killing ability even in an immunosuppressive microenvironment supports the notion of including *ex vivo* derived NK exosomes as a potential tool alongside NK cell based immunotherapy.

## Supplementary Material

Refer to Web version on PubMed Central for supplementary material.

## Acknowledgements

We thank Dr. Hiroyuki Shimada at Children's Hospital Los Angeles for providing electron microscopy images of extracellular vesicles. Dr. Fabbri is supported by the NIH/NCI grant R01CA215753 and by the Pablove Foundation Accelerator Award.

## References

1. Esposito MR, Aveic S, Seydel A, Tonini GP. Neuroblastoma treatment in the post-genomic era. J Biomed Sci 2017;24:14 [PubMed: 28178969]
2. Smith MA, Altekruse SF, Adamson PC, Reaman GH, Seibel NL. Declining childhood and adolescent cancer mortality. Cancer 2014;120:2497–506 [PubMed: 24853691]
3. Brodeur GM, Pritchard J, Berthold F, Carlsen NL, Castel V, Castelberry RP, et al. Revisions of the international criteria for neuroblastoma diagnosis, staging, and response to treatment. J Clin Oncol 1993;11:1466–77 [PubMed: 8336186]

4. Huang M, Weiss WA. Neuroblastoma and MYCN. Cold Spring Harb Perspect Med 2013;3:a014415 [PubMed: 24086065]
5. Otto T, Horn S, Brockmann M, Eilers U, Schüttrumpf L, Popov N, et al. Stabilization of N-Myc is a critical function of Aurora A in human neuroblastoma. Cancer Cell 2009;15:67–78 [PubMed: 19111882]
6. Gustafson WC, Meyerowitz JG, Nekritz EA, Chen J, Benes C, Charron E, et al. Drugging MYCN through an allosteric transition in Aurora kinase A. Cancer Cell 2014;26:414–27 [PubMed: 25175806]
7. Maris JM, Morton CL, Gorlick R, Kolb EA, Lock R, Carol H, et al. Initial testing of the aurora kinase A inhibitor MLN8237 by the Pediatric Preclinical Testing Program (PPTP). Pediatr Blood Cancer 2010;55:26–34 [PubMed: 20108338]
8. Neviani P, Fabbri M. Exosomic microRNAs in the Tumor Microenvironment. Front Med (Lausanne) 2015;2:47 [PubMed: 26258125]
9. Vanichapol T, Chutipongtanate S, Anurathapan U, Hongeng S. Immune Escape Mechanisms and Future Prospects for Immunotherapy in Neuroblastoma. Biomed Res Int 2018;2018:1812535 [PubMed: 29682521]
10. Challagundla KB, Wise PM, Neviani P, Chava H, Murtadha M, Xu T, et al. Exosome-mediated transfer of microRNAs within the tumor microenvironment and neuroblastoma resistance to chemotherapy. J Natl Cancer Inst 2015;107
11. Asgharzadeh S, Salo JA, Ji L, Oberthuer A, Fischer M, Berthold F, et al. Clinical significance of tumor-associated inflammatory cells in metastatic neuroblastoma. J Clin Oncol 2012;30:3525–32 [PubMed: 22927533]
12. Larsen SK, Gao Y, Basse PH. NK cells in the tumor microenvironment. Crit Rev Oncog 2014;19:91–105 [PubMed: 24941376]
13. Tran HC, Wan Z, Sheard MA, Sun J, Jackson JR, Malvar J, et al. TGFBR1 Blockade with Galunisertib (LY2157299) Enhances Anti-Neuroblastoma Activity of the Anti-GD2 Antibody Dinutuximab (ch14.18) with Natural Killer Cells. Clin Cancer Res 2017;23:804–13 [PubMed: 27756784]
14. Xu Y, Sun J, Sheard MA, Tran HC, Wan Z, Liu WY, et al. Lenalidomide overcomes suppression of human natural killer cell anti-tumor functions by neuroblastoma microenvironment-associated IL-6 and TGFβ1. Cancer Immunol Immunother 2013;62:1637–48 [PubMed: 23982484]
15. Castriconi R, Dondero A, Bellora F, Moretta L, Castellano A, Locatelli F, et al. Neuroblastoma-derived TGF-β1 modulates the chemokine receptor repertoire of human resting NK cells. J Immunol 2013;190:5321–8 [PubMed: 23576682]
16. Bottino C, Dondero A, Bellora F, Moretta L, Locatelli F, Pistoia V, et al. Natural killer cells and neuroblastoma: tumor recognition, escape mechanisms, and possible novel immunotherapeutic approaches. Front Immunol 2014;5:56 [PubMed: 24575100]
17. Trotta R, Dal Col J, Yu J, Ciarlariello D, Thomas B, Zhang X, et al. TGF-beta utilizes SMAD3 to inhibit CD16-mediated IFN-gamma production and antibody-dependent cellular cytotoxicity in human NK cells. J Immunol 2008;181:3784–92 [PubMed: 18768831]
18. Bruno A, Ferlazzo G, Albini A, Noonan DM. A think tank of TINK/TANKs: tumor-infiltrating/tumor-associated natural killer cells in tumor progression and angiogenesis. J Natl Cancer Inst 2014;106:dju200 [PubMed: 25178695]
19. Xu J, Lamouille S, Derynck R. TGF-beta-induced epithelial to mesenchymal transition. Cell Res 2009;19:156–72 [PubMed: 19153598]
20. Lynch J, Fay J, Meehan M, Bryan K, Watters KM, Murphy DM, et al. MiRNA-335 suppresses neuroblastoma cell invasiveness by direct targeting of multiple genes from the non-canonical TGF-β signalling pathway. Carcinogenesis 2012;33:976–85 [PubMed: 22382496]
21. Shao JB, Gao ZM, Huang WY, Lu ZB. The mechanism of epithelial-mesenchymal transition induced by TGF-β1 in neuroblastoma cells. Int J Oncol 2017;50:1623–33 [PubMed: 28393230]
22. Jong AY, Wu CH, Li J, Sun J, Fabbri M, Wayne AS, et al. Large-scale isolation and cytotoxicity of extracellular vesicles derived from activated human natural killer cells. J Extracell Vesicles 2017;6:1294368 [PubMed: 28326171]

23. Lugini L, Cecchetti S, Huber V, Luciani F, Macchia G, Spadaro F, et al. Immune surveillance properties of human NK cell-derived exosomes. J Immunol 2012;189:2833–42 [PubMed: 22904309]
24. Zhu L, Kalimuthu S, Gangadaran P, Oh JM, Lee HW, Baek SH, et al. Exosomes Derived From Natural Killer Cells Exert Therapeutic Effect in Melanoma. Theranostics 2017;7:2732–45 [PubMed: 28819459]
25. Reynolds CP, Tomayko MM, Donner L, Helson L, Seeger RC, Triche TJ, et al. Biological classification of cell lines derived from human extra-cranial neural tumors. Prog Clin Biol Res 1988;271:291–306 [PubMed: 3406003]
26. Wang X, Lee DA, Wang Y, Wang L, Yao Y, Lin Z, et al. Membrane-bound interleukin-21 and CD137 ligand induce functional human natural killer cells from peripheral blood mononuclear cells through STAT-3 activation. Clin Exp Immunol 2013;172:104–12 [PubMed: 23480190]
27. Subramanyam D, Lamouille S, Judson RL, Liu JY, Bucay N, Derynck R, et al. Multiple targets of miR-302 and miR-372 promote reprogramming of human fibroblasts to induced pluripotent stem cells. Nat Biotechnol 2011;29:443–8 [PubMed: 21490602]
28. Zawel L, Dai JL, Buckhaults P, Zhou S, Kinzler KW, Vogelstein B, et al. Human Smad3 and Smad4 are sequence-specific transcription activators. Mol Cell 1998;1:611–7 [PubMed: 9660945]
29. Huang X, Schwind S, Yu B, Santhanam R, Wang H, Hoellerbauer P, et al. Targeted delivery of microRNA-29b by transferrin-conjugated anionic lipopolyplex nanoparticles: a novel therapeutic strategy in acute myeloid leukemia. Clin Cancer Res 2013;19:2355–67 [PubMed: 23493348]
30. Lötvall J, Hill AF, Hochberg F, Buzás EI, Di Vizio D, Gardiner C, et al. Minimal experimental requirements for definition of extracellular vesicles and their functions: a position statement from the International Society for Extracellular Vesicles. J Extracell Vesicles 2014;3:26913 [PubMed: 25536934]
31. Zhang W, Yu Y, Hertwig F, Thierry-Mieg J, Thierry-Mieg D, Wang J, et al. Comparison of RNA-seq and microarray-based models for clinical endpoint prediction. Genome Biol 2015;16:133 [PubMed: 26109056]
32. Ikeda H, Iehara T, Tsuchida Y, Kaneko M, Hata J, Naito H, et al. Experience with International Neuroblastoma Staging System and Pathology Classification. Br J Cancer 2002;86:1110–6 [PubMed: 11953858]
33. Wang F, Jiang H, Wang S, Chen B. Dual Functional MicroRNA-186–5p Targets both FGF2 and RelA to Suppress Tumorigenesis of Glioblastoma Multiforme. Cell Mol Neurobiol 2017
34. Cao C, Sun D, Zhang L, Song L. miR-186 affects the proliferation, invasion and migration of human gastric cancer by inhibition of Twist1. Oncotarget 2016;7:79956–63 [PubMed: 27835599]
35. Huang T, She K, Peng G, Wang W, Huang J, Li J, et al. MicroRNA-186 suppresses cell proliferation and metastasis through targeting MAP3K2 in non-small cell lung cancer. Int J Oncol 2016;49:1437–44 [PubMed: 27498924]
36. Ruan T, He X, Yu J, Hang Z. MicroRNA-186 targets Yes-associated protein 1 to inhibit Hippo signaling and tumorigenesis in hepatocellular carcinoma. Oncol Lett 2016;11:2941–5 [PubMed: 27073580]
37. Liu Z, Zhang G, Yu W, Gao N, Peng J. miR-186 inhibits cell proliferation in multiple myeloma by repressing Jagged1. Biochem Biophys Res Commun 2016;469:692–7 [PubMed: 26679605]
38. He W, Feng J, Zhang Y, Wang Y, Zang W, Zhao G. microRNA-186 inhibits cell proliferation and induces apoptosis in human esophageal squamous cell carcinoma by targeting SKP2. Lab Invest 2016;96:317–24 [PubMed: 26568291]
39. Cui G, Cui M, Li Y, Liang Y, Li W, Guo H, et al. MiR-186 targets ROCK1 to suppress the growth and metastasis of NSCLC cells. Tumour Biol 2014;35:8933–7 [PubMed: 24894676]
40. Chen F, Zhou C, Lu Y, Yuan L, Peng F, Zheng L, et al. [Expression of hsa-miR-186 and its role in human colon carcinoma cells]. Nan Fang Yi Ke Da Xue Xue Bao 2013;33:654–60 [PubMed: 23688982]
41. Wang F, Jiang H, Wang S, Chen B. Dual Functional MicroRNA-186–5p Targets both FGF2 and RelA to Suppress Tumorigenesis of Glioblastoma Multiforme. Cellular and Molecular Neurobiology 2017:1–10 [PubMed: 26935061]

42. Dorrance AM, Neviani P, Ferenchak GJ, Huang X, Nicolet D, Maharry KS, et al. Targeting leukemia stem cells in vivo with antagomiR-126 nanoparticles in acute myeloid leukemia. Leukemia 2015;29:2143–53 [PubMed: 26055302]
43. Challagundla KB, Fanini F, Vannini I, Wise P, Murtadha M, Malinconico L, et al. microRNAs in the tumor microenvironment: solving the riddle for a better diagnostics. Expert Rev Mol Diagn 2014;14:565–74 [PubMed: 24844135]
44. Ara T, Nakata R, Sheard MA, Shimada H, Buettner R, Groshen SG, et al. Critical role of STAT3 in IL-6-mediated drug resistance in human neuroblastoma. Cancer Res 2013;73:3852–64 [PubMed: 23633489]
45. Metelitsa LS, Wu HW, Wang H, Yang Y, Warsi Z, Asgharzadeh S, et al. Natural killer T cells infiltrate neuroblastomas expressing the chemokine CCL2. J Exp Med 2004;199:1213–21 [PubMed: 15123743]
46. Mei H, Lin ZY, Tong QS. The roles of microRNAs in neuroblastoma. World J Pediatr 2014;10:10–6 [PubMed: 24464658]
47. Lu S, Wang MS, Chen PJ, Ren Q, Bai P. miRNA-186 inhibits prostate cancer cell proliferation and tumor growth by targeting YY1 and CDK6. Exp Ther Med 2017;13:3309–14 [PubMed: 28587405]
48. Jiao D, Wu M, Ji L, Liu F, Liu Y. microRNA-186 Suppresses Cell Proliferation and Metastasis Through Targeting Sentrin Specific Protease 1 in Renal Cell Carcinoma. Oncol Res 2017
49. Zhang JJ, Wang DD, Du CX, Wang Y. Long Noncoding RNA ANRIL Promotes Cervical Cancer Development By Acting as a Sponge of miR-186. Oncol Res 2017
50. Myatt SS, Wang J, Monteiro LJ, Christian M, Ho KK, Fusi L, et al. Definition of microRNAs that repress expression of the tumor suppressor gene FOXO1 in endometrial cancer. Cancer Res 2010;70:367–77 [PubMed: 20028871]
51. Qiu H, Yuan S, Lu X. miR-186 suppressed CYLD expression and promoted cell proliferation in human melanoma. Oncol Lett 2016;12:2301–6 [PubMed: 27698793]
52. Islam F, Gopalan V, Vider J, Wahab R, Ebrahimi F, Lu CT, et al. MicroRNA-186–5p overexpression modulates colon cancer growth by repressing the expression of the FAM134B tumour inhibitor. Exp Cell Res 2017;357:260–70 [PubMed: 28549913]
53. Kerkelä E, Ala-aho R, Klemi P, Grénman S, Shapiro SD, Kähäri VM, et al. Metalloelastase (MMP-12) expression by tumour cells in squamous cell carcinoma of the vulva correlates with invasiveness, while that by macrophages predicts better outcome. J Pathol 2002;198:258–69 [PubMed: 12237887]
54. Klupp F, Neumann L, Kahlert C, Diers J, Halama N, Franz C, et al. Serum MMP7, MMP10 and MMP12 level as negative prognostic markers in colon cancer patients. BMC Cancer 2016;16:494 [PubMed: 27431388]
55. Park SJ, Park CJ, Kim S, Jang S, Chi HS, Kim MJ, et al. Detection of bone marrow metastases of neuroblastoma with immunohistochemical staining of CD56, chromogranin A, and synaptophysin. Appl Immunohistochem Mol Morphol 2010;18:348–52 [PubMed: 20216406]

**Statement of Significance:** Findings highlight the therapeutic potential of NK cell-derived exosomes containing the tumor suppressor miR-186 that inhibits growth, spreading, and TGFβ-dependent immune escape mechanisms in neuroblastoma.

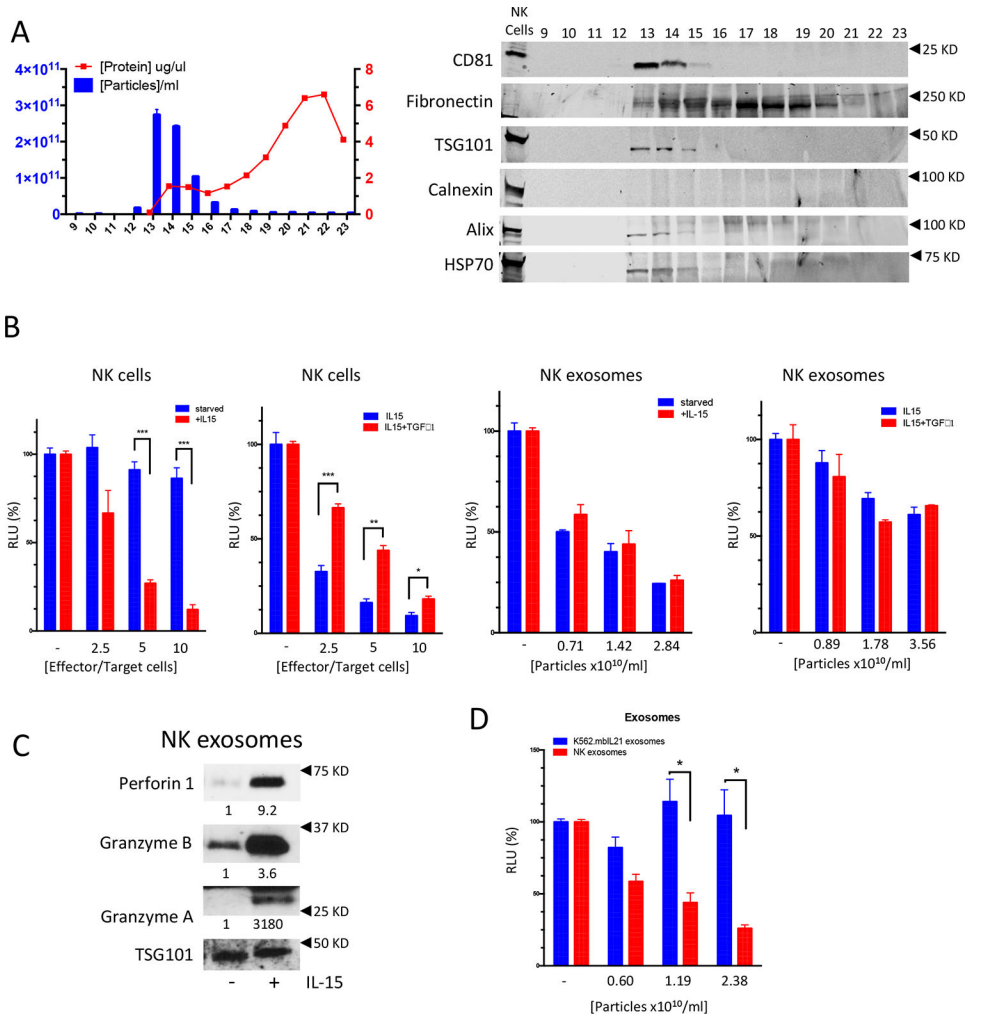


**Figure 1.**

**(A)** *Left*: particle number (by nanosight tracking analysis) and total protein concentration in SEC fractions 9 through 23. *Right*: immunoblotting showing the expression of CD81 Fibronectin, TSG101, Calnexin, Alix and HSP70 in SEC fractions 9 through 23; NK cell lysate (lane 1) was used as a control. **(B)** Cytotoxic potential of NK cells or NK exosomes assessed by luciferase reporter cytotoxicity assays: CHLA-136-Fluc cells (target cells) were exposed to increasing numbers of NK cells (effector cells) for 6 hours or increasing NK exosome particle numbers for 24 hours. NK cells were starved from growth factors or rhIL-15 activated for at least 48h or inhibited by TGFβ1 treatment for 4 days; exosomes were isolated from the corresponding supernatants by SEC. Cytotoxicity is expressed as a percent change of Relative Luminometry Units (RLU) compared to the untreated control **(C)** Immunoblotting showing the expression of Perforin 1, Granzyme A, Granzyme B in NK exosomes derived from NK cells starved from growth factors or rhIL-15 treated for 48h; densitometry numbers underneath blots are expressed as arbitrary units normalized to levels of TSG101, used as loading control for the exosomes. **(D)** Comparison of cytotoxic potential of exosomes derived from NK cells or K562.mbIL21 cells. * P<0.05, **P<0.01, ***P<0.001. Student's t-test, two-tailed.

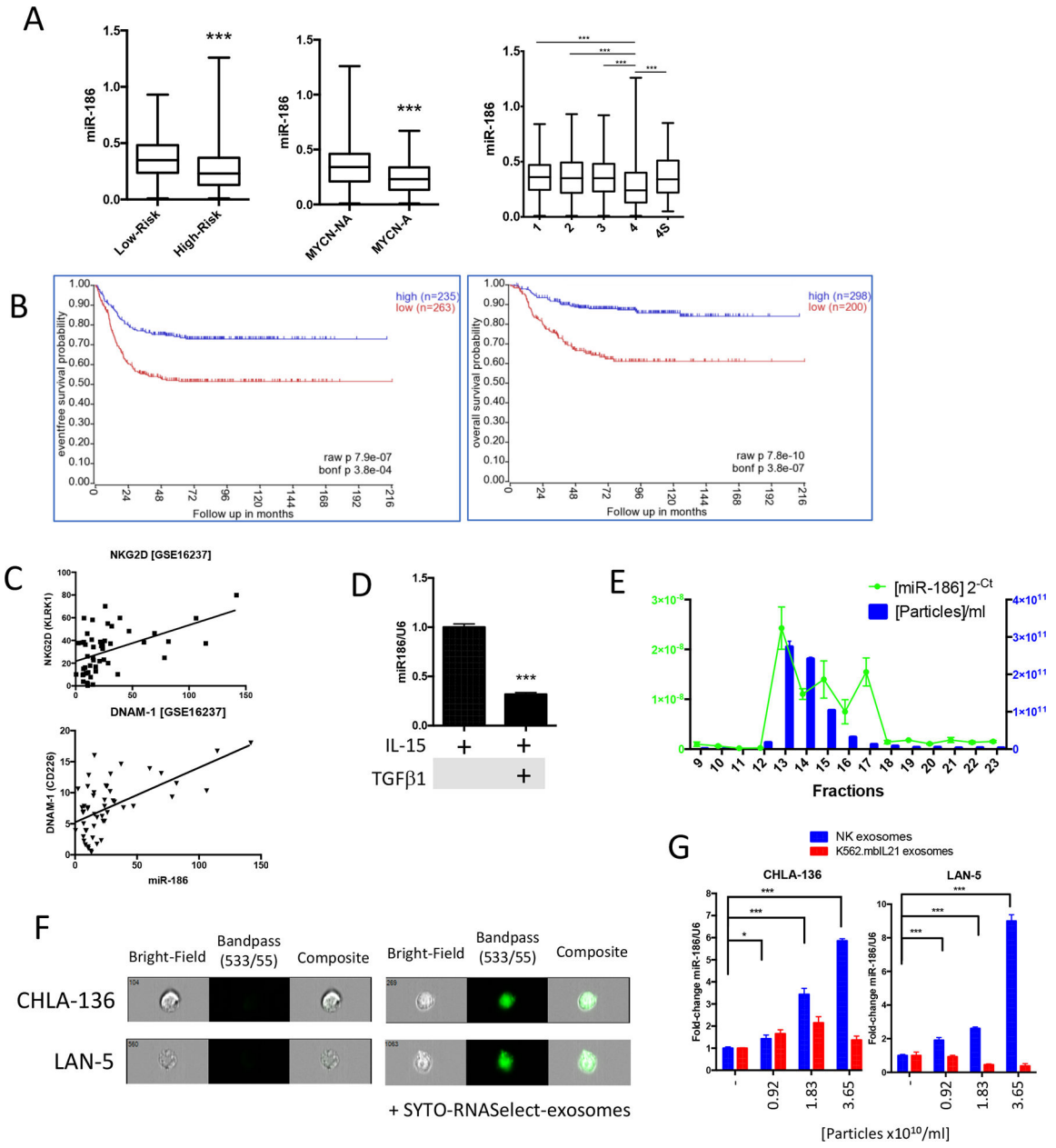


**Figure 2.**

**(A)** Expression of miR-186 in the GSE62564 RNA-seq dataset representing 498 neuroblastoma patients stratified by: low-risk vs high-risk; MYCN non amplified (NA) vs amplified (A); INSS staging. **(B)** miR-186 based event-free survival *(left)* and overall survival *(right)* probability analysis (n=498). **(C)** Correlation between miR-186 and NKG2D (KLRK1, $r^2$=0.495; **) and DNAM-1 (CD226, $r^2$=0.602; ***) in 61 patients represented in the GSE16237 Affymetrix gene expression array dataset. **(D)** Detection of miR-186 by qRT-PCR in NK cells treated for 96 hours with rhIL-15 (100ng/ml) and rhTGFβ1 (10ng/ml) as indicated. **(E)** Particle number (by nanosight tracking analysis), total protein concentration and miR-186 expression (by qRT-PCR) in SEC fractions 9 through 23. **(F)** Delivery of the exosomal RNA cargo into CHLA-136 and LAN-5 cells exposed to SYTO-RNASelect-

labeled NK exosomes for 18h. **(G)** Detection of miR-186 by qRT-PCR in CHLA-136 or LAN-5 cells exposed to NK or K562.mbIL21 exosomes for 18 hours. * P<0.05, **P<0.01, ***P<0.001. Student's t-test, two-tailed.

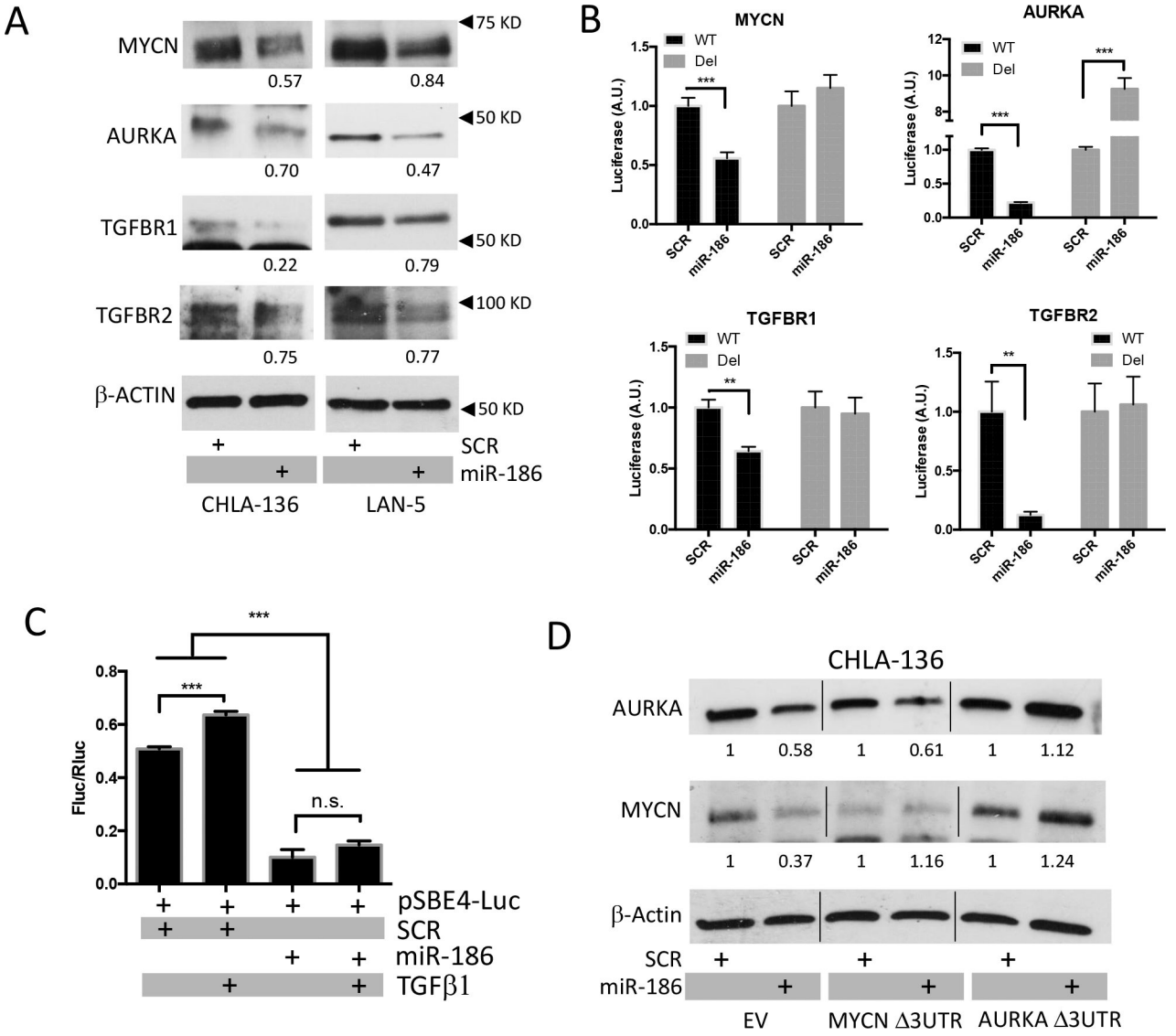


**Figure 3.**

**(A)** Immunoblotting for MYCN, AURKA, TGFBR1 and TGFBR2 in CHLA-136 and LAN-5 cells treated with Dotap-miR-186 or Dotap-Scr for 48 or 72 hours, respectively; densitometry numbers underneath blots are expressed as arbitrary units normalized to levels of β-ACTIN, used as loading control. **(B)** Luciferase reporter assays of CHLA-255 cells electroporated with the mature miR-186 (or a scrambled SCR control) and the psiCHECK-2 vector carrying the wild-type (WT) or seed-sequence deleted (Del) 3'UTR of MYCN, AURKA, TGFBR1 or TGFBR2. **(C)** Luciferase reporter assay of CHLA-255 cells electroporated with the mature miR-186 (or a scrambled SCR control) and the pSBE4-luc vector and treated with TGFβ1 where indicated. **(D)** Immunoblotting for MYCN and AURKA in CHLA-136 cells transduced with the lentiviral vectors containing the full length coding sequence of MYCN or AURKA without their (Δ3UTR) and treated with Dotap-miR-186 or Dotap-Scr for 24 hours; densitometry numbers underneath blots are expressed

as arbitrary units normalized to levels of β-ACTIN, used as loading control. **P<0.01, ***P<0.001. Student's t-test, two-tailed.

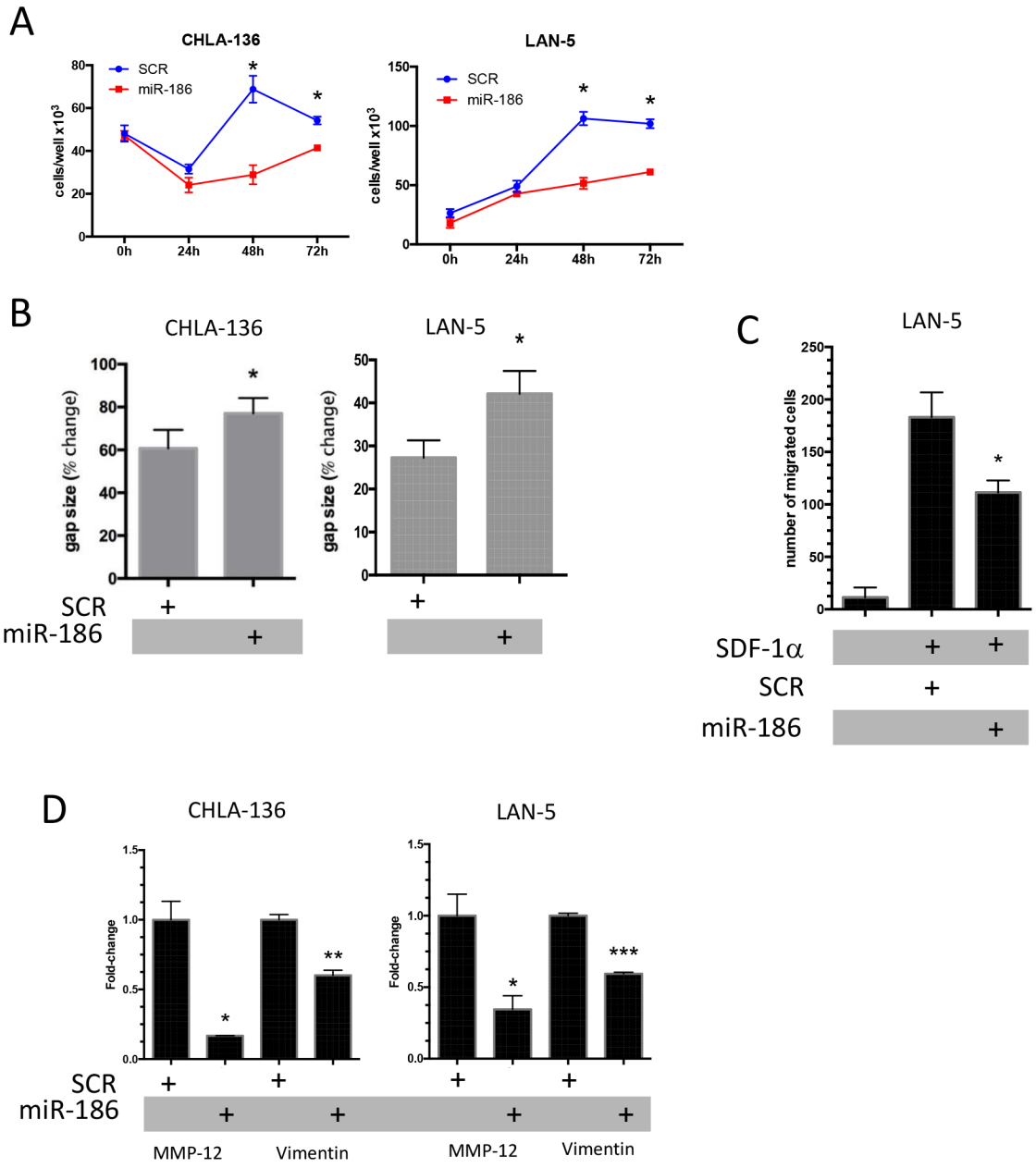


**Figure 4.**

**(A)** Growth curves of CHLA-136 and LAN-5 cells treated with Dotap-miR-186 or Dotap-Scr and followed for up to 72 hours. **(B)** Wound-healing assays of CHLA-136 and LAN-5 cells treated with Dotap-miR-186 or Dotap-Scr. The gap size after 6 days is expressed as a percentage of the gap size at time zero. **(C)** Boyden chamber migration assay of LAN-5 cells treated with Dotap-miR-186 or Dotap-Scr and exposed to SDF1a for 4 hours; the absolute number of migrated cells is reported. **(D)** Expression of MMP-12 and Vimentin by SYBR-green qRT-PCR in CHLA-136 or LAN-5 cells treated with Dotap-miR-186 or Dotap-Scr. * P<0.05, **P<0.01, ***P<0.001. Student's t-test, two-tailed.

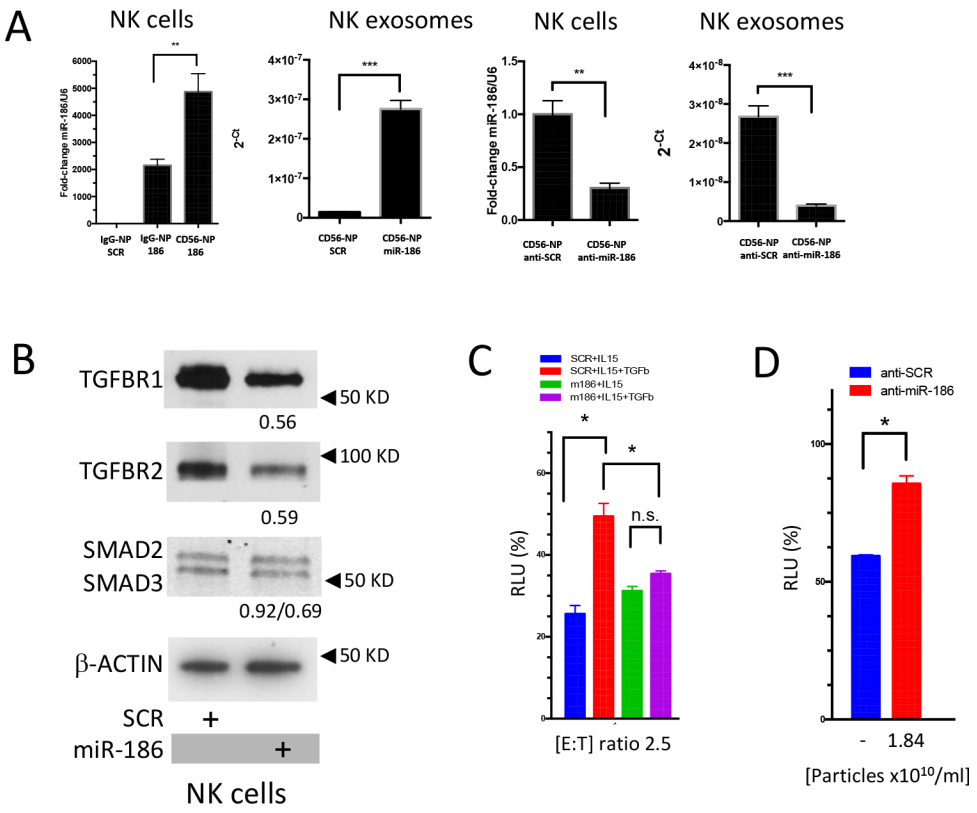


**Figure 5.**

**(A)** Expression of miR-186 by qRT-PCR in NK cells or NK exosomes exposed to IgG-control or CD56-labeled nanoparticles loaded with the mimic miR-186 (50nM) or the antagomiR anti-miR-186 (50nM) or the respective scrambled controls. **(B)** Immunoblotting showing the expression of TGFBR1, TGFBR2, SMAD2 and SMAD3 in NK cells treated with CD56-labeled nanoparticles loaded with the mimic miR-186 or its scrambled control; densitometry numbers underneath blots are expressed as arbitrary units normalized to levels of β-ACTIN, used as loading control. **(C)** 6 hour cytotoxicity assay of CHLA-136-Fluc cells exposed to NK cells previously treated (4 days) with CD56-labeled nanoparticles and IL-15, and TGFβ1, as indicated. **(D)** 24 hour cytotoxicity assay of CHLA-136-Fluc cells exposed to NK exosomes derived from the supernatant of NK cells treated with CD56-labeled nanoparticles loaded with the antagomiR anti-miR-186 (50nM) or its scrambled control. * P<0.05, **P<0.01, ***P<0.001. Student's t-test, two-tailed.

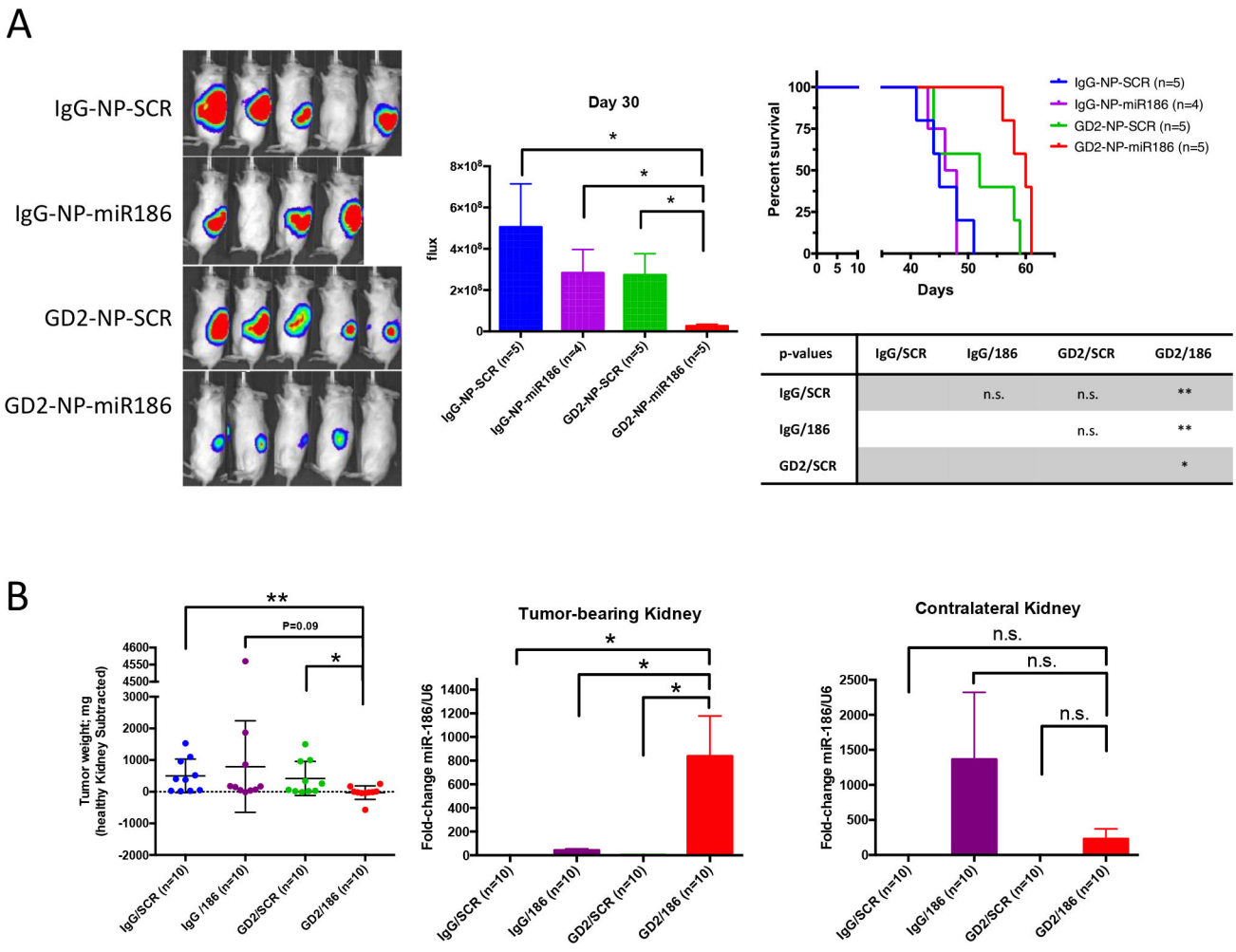


**Figure 6.**

**(A)** Bioluminescence imaging (*left*) and signal quantification (*middle*) of mice 30 days after orthotopic transplantation of CHLA-136-Fluc cells and treated as indicated. *Right:* Kaplan-Meier survival analysis. GD2-NP-miR186 median survival: 60 days, IgG-NP-Scr median survival: 45 days, IgG-NP-miR-186 median survival: 47 days, and GD2-NP-Scr median survival: 52 days. **(B)** *Left*: Tumor weight analysis of tumor-bearing kidneys in mice euthanized 30 days after orthotopic injection of CHLA-136-Fluc cells and 26 days of treatment with the indicated nanoparticles. The weight of the impacted kidney was subtracted from the weight of the healthy contralateral kidney. *Middle and right*: expression of miR-186 by qRT-PCR in homogenates from the tumor-bearing and the contralateral healthy kidney. * P<0.05, **P<0.01. Student's t-test, two-tailed.

**TABLE 1**

*In-silico* predicted targets of miRs found in NK exosomes

| | | MYCN | TGFBR1 | SMAD2 | SMAD3 | AURKA |
|---|---|---|---|---|---|---|
| *hsa-miR-17-002308* | 24.1 | X | X | X | X | |
| *hsa-miR-146a-000468* | 24.4 | | X | X | X | |
| *hsa-miR-155-002623* | 24.6 | | X | X | X | |
| *hsa-miR-222-002276* | 24.8 | | X | X | | |
| *hsa-miR-16-000391* | 25.4 | | X | X | X | |
| *hsa-miR-19b-000396* | 25.5 | X | X | X | | |
| *hsa-miR-484-001821* | 25.7 | X | X | X | X | |
| *hsa-miR-146b-001097* | 25.9 | | X | X | X | X |
| *hsa-miR-24-000402* | 26.0 | | X | X | | X |
| *hsa-miR-150-000473* | 26.5 | X | X | | X | X |
| *hsa-miR-342-3p-002260* | 26.8 | | | X | X | |
| **hsa-miR-186-002285** | **27.2** | **X** | **X** | **X** | **X** | **X** |
| *hsa-miR-29a-002112* | 27.3 | X | | X | X | |
| *hsa-miR-20a-002112* | 27.4 | X | X | X | X | |
| *hsa-miR-618-001593* | 27.7 | | X | X | X | |
| *hsa-miR-411-001610* | 27.8 | | | X | X | |
| *hsa-miR-142-3p-000464* | 28.0 | | X | X | | |
| *hsa-miR-320-002277* | 28.1 | | X | X | X | |
| *hsa-miR-518b-001156* | 28.4 | | X | | | |
| *hsa-miR-19a-000395* | 28.5 | X | X | | | |
| *hsa-miR-454-002323* | 28.5 | | | X | | |
| *hsa-miR-223-002295* | 28.7 | | | X | X | |